Nuclear Instruments and Methods in Physics Research A ∎ (∎∎∎∎) ∎∎∎–∎∎∎

Contents lists available at ScienceDirect

Nuclear Instruments and Methods in Physics Research A

journal homepage: www.elsevier.com/locate/nima

Recent progress of MPPC-based scintillation detectors in high precision X-ray and gamma-ray imaging

J. Kataoka [a,*], A. Kishimoto [a], T. Fujita [a], T. Nishiyama [a], Y. Kurei [a], T. Tsujikawa [a], T. Oshima [a], T. Taya [a], Y. Iwamoto [a], H. Ogata [a], H. Okochi [a], S. Ohsuka [b], H. Ikeda [c], S. Yamamoto [d]

[a] Research Institute for Science and Engineering, Waseda University, 3-4-1 Okubo, Shinjuku, Tokyo 169-8555, Japan
[b] Central Research Laboratory, Hamamatsu Photonics K.K., 5000, Hirakuchi, Hamakita-ku, Hamamatsu, Shizuoka, Japan
[c] ISAS/JAXA, 3-1-1, Yoshinodai, Chuo-ku, Sagamihara-shi, Kanagawa, Japan
[d] Department of Radiological and Medical Laboratory Sciences, Nagoya University, 65, Tsurumai-cho, Showa-ku, Nagoya-shi, Aichi, Japan

ARTICLE INFO

Keywords:
Multi-pixel photon counter (MPPC)
Scintillator
Next generation PET
Compton camera

ABSTRACT

The multi-pixel photon counter (MPPC) is a promising light sensor for various applications, not only in physics experiments but also in nuclear medicine, industry, and even high-energy astrophysics. In this paper, we present the current status and most recent progress of the MPPC-based scintillation detectors, such as (1) a high-precision X-ray and gamma-ray spectral image sensor, (2) next-generation PET detectors with MRI, TOF, and DOI measurement capabilities, and (3) a compact gamma camera for environmental radiation surveys. We first present a new method of fabricating a Ce:GAGG scintillator plate (1 or 2 mm thick) with ultra-fine resolution (0.2 mm/pixel), cut using a dicing saw to create 50 μm wide micro-grooves. When the plate is optically coupled with a large-area MPPC array, excellent spatial resolution of 0.48 mm (FWHM) and energy resolution of 14% (FWHM) are obtained for 122 keV gamma rays. Hence, the detector can act as a convenient "multi-color" imaging device that can potentially be used for future SPECT and photon-counting CT. We then show a prototype system for a high-resolution MPPC-based PET scanner that can realize $\simeq 1$ mm (FWHM) spatial resolution, even under a strong magnetic field of 4.7 T. We develop a front-end ASIC intended for future TOF-PET scanner with a 16-channel readout that achieves a coincidence time resolution of 489 ps (FWHM). A novel design for a module with DOI-measurement capability for gamma rays is also presented by measuring the pulse height ratio of double-sided MPPCs coupled at both ends of scintillation crystal block. Finally, we present the concept of a two-plane Compton camera consisting of Ce:GAGG scintillator arrays coupled with thin MPPC arrays. As a result of the thin and compact features of the MPPC device, the camera not only achieves a small size ($14 \times 14 \times 15$ cm^3) and light weight (1.9 kg) but also excellent sensitivity, compared to the conventional PMT-based pinhole camera used in Fukushima. Finally, we briefly describe a new product recently developed in conjunction with Hamamatsu Photonics K.K. that offers improved sensitivity and angular resolution of $\Delta\theta \sim 8^\circ$ (FWHM) at 662 keV, by incorporating DOI-segmented scintillator arrays.

1. Introduction

The multi-pixel photon counter (MPPC), also referred to as a silicon photomultiplier (Si-PM), was developed by Hamamatsu Photonics K.K. (hereafter, Hamamatsu) and is a solid-state photon counting device consisting of hundreds to over ten thousand avalanche photodiode (APD) pixels in the Geiger-mode. Ref. [1] gives details of the design concept, operating mode and basic performance of MPPCs.

As shown in Fig. 1, the MPPC has many advantages which are similar to those of conventional linear-mode APDs (e.g. [2,3]), such as insensitivity to magnetic fields, robustness and compactness, and high signal amplification gain up to the million level (making it comparable to photo-multiplier [PMT] gain). However, the dynamic range of the MPPC is often limited by the number of Geiger-mode APD pixels comprised in the device, resulting in a non-linear response to the number of incident photons. Moreover, thermal electrons often trigger a Geiger discharge, thereby making the substantial contamination of dark counts a possible problem, especially for weak photon detection. The technical optimization of the MPPC device is still underway, but the latest products successfully achieve a substantial

* Corresponding author.
E-mail address: kataoka.jun@waseda.jp (J. Kataoka).

http://dx.doi.org/10.1016/j.nima.2014.11.004
0168-9002/

reduction of dark counts and improved photon detection efficiency, in addition to pixel size miniaturization to extend the device's dynamic range [4].

Hamamatsu has released a variety of MPPC products since 2008. Particularly noteworthy are position-sensitive arrays (e.g., 2×2 or 4×4 matrices of MPPC pixels) that may replace conventional multi-anode PMTs in certain applications. The first MPPC array (released in 2010) was an assembly of discrete 3×3 mm^2 pixels (see, Fig. 1). Then, in 2012, a large-area, monolithic MPPC array fabricated in 3-side buttable packages was released. This MPPC array has already been tested for various applications [5–7] and is a key device that will be demonstrated in later sections of this paper. Finally, through-silicon via (TSV) technology enables the production of a large active area and less dead space in 4-side buttable package of the MPPC-array and, in 2014, Hamamatsu took on the challenge of fabricating various types of TSV-MPPCs, arranged into 8×8 or 16×16 channels (ch) [8].

Given the current development status, various MPPC applications are now being proposed, not only in physics experiments but also in nuclear medicine, industry, and even high-energy astrophysics. In this paper, we focus on reviewing the current status and most recent progress of MPPC-based scintillation detectors by considering applications such as a high-precision X-ray and gamma-ray spectral image sensor (in Section 2), next-generation PET detectors having magnetic-resonance imaging (MRI), time-of-flight (TOF) , and depth-of-interaction (DOI) measurement capabilities (in Section 3), and a compact gamma camera for environmental radiation surveys (in Section 4).

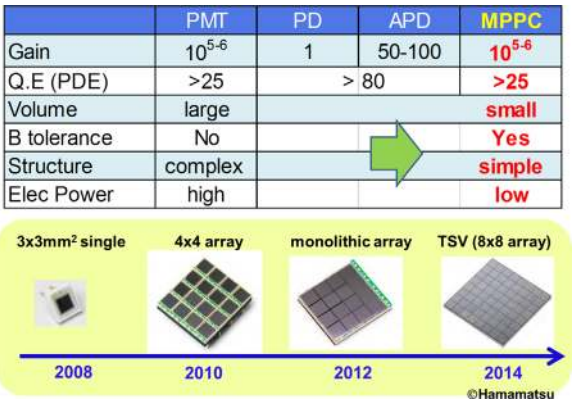

Fig. 1. (*Upper*) Basic properties and advantages of MPPC in comparison with conventional PMTs, PDs and APDs. (*Bottom*) A brief history of MPPC development and related products developed with Hamamatsu Photonics K.K.

2. Multi-color, ultra-fine resolution scintillation camera

X-ray and gamma-ray imaging techniques using fine scintillator arrays coupled with optical sensors are commonly used in medicine, physics experiments, and homeland security. For example, gamma-cameras based on PMTs have a long history, depending on the scintillator used and detector arrangement. In some cases, spatial resolutions at the sub-millimeter level has been recorded (e.g., [12,13]), but this is still far from the 0.1 to 0.2 mm resolution possible with flat panel X-ray detectors (FPD; e.g. [9]). However, FPDs are minimally sensitive to gamma rays, high in cost, and unsuitable for

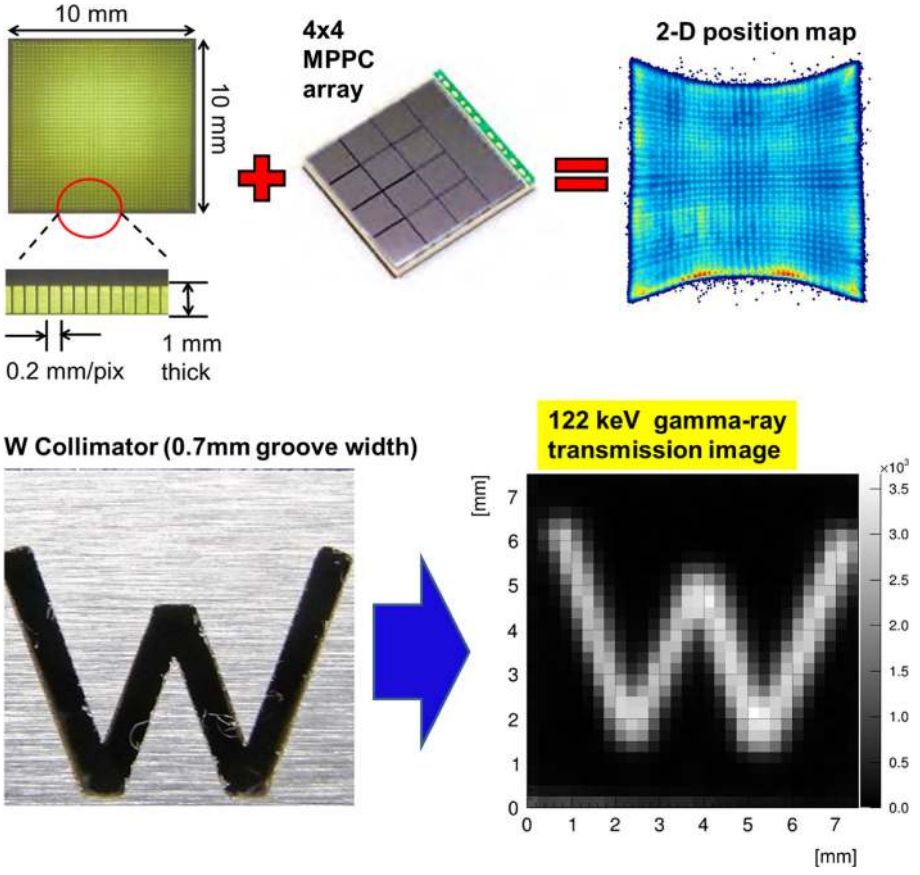

Fig. 2. (*Top*) Photo of diced Ce:GAGG scintillator array to be coupled with MPPC array, with a flood map taken with a ^{60} Co source shown on the right. (*Bottom*) Tungsten collimator (with a 0.7 mm-wide W-shaped groove) and resultant image, taken at 122 keV.

Please cite this article as: J. Kataoka, et al., Nuclear Instruments & Methods in Physics Research A (2014), http://dx.doi.org/10.1016/j.nima.2014.11.004

photon counting or measuring spectra. Traditional PMTs coupled with pixelated scintillator arrays are often used in single photon emission computed tomography (SPECT) and positron emission tomography (PET) applications, although their resolution is typically limited to a few mm (FWHM) or greater (~10 mm for SPECT), due to the pixel size of the scintillator fabricated in the array. Very recently, sub-millimeter spatial resolution based on newly developed APD or MPPC arrays has been reported for PET scanners, but the resolution is still limited to the 0.8–1.2 mm level, partly because of restrictions due to the positron range [10,11].

In our new approach, a Ce:GAGG scintillator plate (10×10 mm^2) of 1.0 mm thickness is cut using a dicing saw to create 50 μm wide micro-grooves, with a resultant thickness of 0.1 mm [2]. This yields a Ce:GAGG array featuring 0.25 mm pitch and 40×40 pixels of 0.2 mm each, as shown in the top left in Fig. 2. Of course, we can choose any kind of scintillator in place of Ce:GAGG, as blade dicing is a very common technique used to cut semiconductor wafers. This scintillator array is optically coupled with 4×4 MPPC array, having a photo-sensitive area of 3×3 mm^2 and 60×60 pixel APDs in the Geiger mode, arranged with 50 μm between each MPPC pixel (Hamamatsu S11830-3344MB; shown in the top center of Fig. 2). The top right of Fig. 2 is a flood map, while the bottom shows the results of an imaging test for 122 keV gamma rays using a thin tungsten collimator (with a "W"-shaped groove that was 0.7 mm in width) placed on the detectors [14].

We obtained excellent spatial resolution of 0.48 mm (FWHM), but this could have be further improved (down to ~0.2 mm) using the finer 1 mm pixel TSV-MPPC arrays now being developed by Hamamatsu. As another advantage of using diced scintillator array, we can also record the energy spectra of incident gamma rays (as shown in Fig. 3) together with a high-resolution image. The recorded energy resolution is 14% (FWHM) for 122 keV gamma-rays. As a result, this simple configuration of scintillator plate coupled with a MPPC array acts as a "multi-color" imaging device that could be easily applied to future SPECT and photon-counting CT. In addition to the new type of TSV-MPPC arrays being developed, we are now fabricating a thicker Ce:GAGG scintillator plate with dimensions of 20×20 mm^2 and a thickness of 2.0 mm, which is cut using a dicing saw with 0.15 mm pitch to achieve up to ~0.2 mm resolution. Thus, it is comparable with FPD image resolution.

3. MPPC-based PET scanner

3.1. Prototype gantry for small animals

MPPCs are also attractive candidates to replace conventional PMTs in PET scanners. In particular, there are high expectations for the future application of MPPCs to MRI-PET, TOF-PET and DOI-PET. To date, various groups have proposed MPPC-based (or Si-PM based) PET detectors (e.g. [7,11,15,16]). The top of Fig. 4 shows the prototype MPPC-based PET gantry (70 mm inner diameter, 190 mm outer diameter) developed by our group for the scanning of small animals such as mice. The gantry consists of eight modules of 4×4 MPPC arrays, coupled with a Ce:LYSO scintillator array fabricated into 16×16 matrices of $0.5 \times 0.5 \times 10$ mm^3 pixels. Since there are only eight detector units, a somewhat low number in this test gantry, we captured the image three times at specific position, obtained by rotating the gantry to 0°, 15° and 30°. The data was then interpolated.

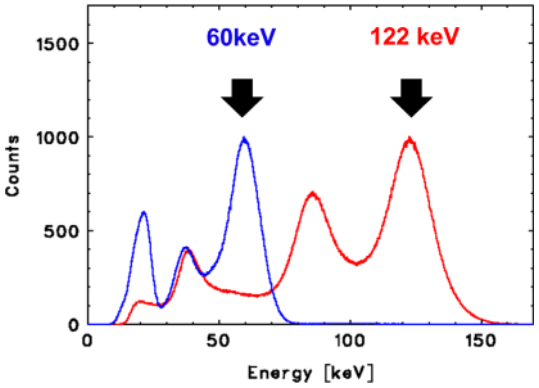

Fig. 3. Gamma-ray spectra taken with Ce:GAGG scintillator plates shown in Fig. 2. The energy resolutions were 24% (FWHM) and 14% (FWHM) for 60 keV and 122 keV gamma rays, respectively.

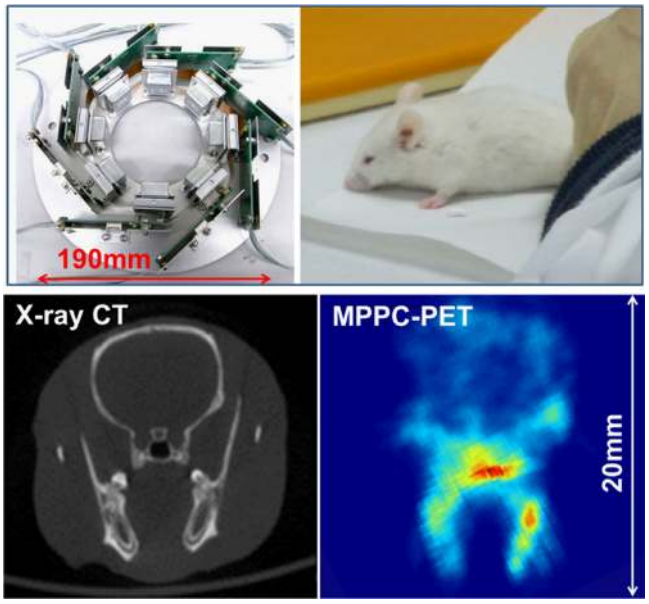

Fig. 4. (*Top*) Photo of prototype MPPC-based PET gantry developed in this paper and a test mouse. (*Bottom*) PET image of mouse brain taken with MPPC-based PET gantry, as compared with corresponding X-ray CT image.

Output signals from each MPPC array were fed into a dedicated coincidence data acquisition (DAQ) system (developed by ESPEC Techno Corp.) after four position-encoded analog outputs were compiled [7]. The compiled signals were digitized by a 100-MHz analog-to-digital converter (ADC). If the timing signals from the MPPC-arrays coincidence were within a time window of 20 ns and their energies were within the range of 511 ± 100 keV, the HIT position, timing were stored in a memory to be used for the creation of list mode data. The bottom right of Fig. 4 shows a sample PET image of a mouse brain as reconstructed from an F-18-NaF study, while the bottom left of this image is the corresponding X-ray CT image for comparison. Although the image is slightly noisy because of the incomplete field of view, the mouse skull structure is clearly observable, with a spatial resolution of up to ~1 mm (FWHM) for the PET image.

3.2. New challenges for MRI-PET

To test the applicability of MPPC arrays to future MRI-PET scanners, we first demonstrated the performance of a pair of modules consisting of 4×4 MPPC-arrays optically coupled with Ce:LYSO scintillators fabricated into 12×12 matrices of 1×1 mm^2 pixels, where a pair of MPPC-PET module was arranged in a ring (90 mm diameter) and positioned around the RF coil of the 4.7-T MRI systems. As detailed in Ref. [17], only slight degradation was found in the spatial resolution of the PET images. The *x*-direction resolutions for a point source (^{22}Na) when the MPPC-PET module is inside the MRI under fast spin echo (FSE) and gradient echo (GE) were $1.65 \pm$

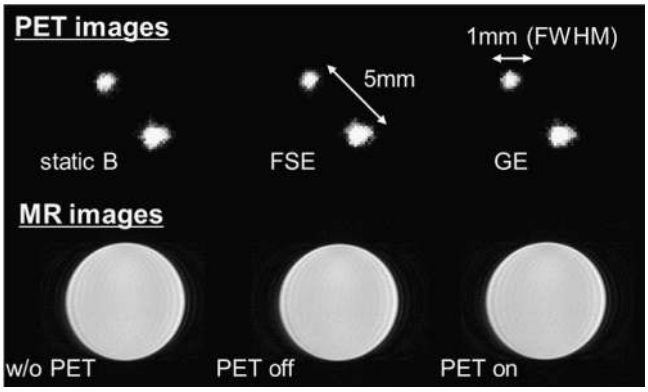

Fig. 5. Comparison of PET images (*top*) and MR images (*bottom*) taken under various conditions to check interference between PET and MRI for future MRI-PET scanners.

0.07 mm (FWHM) and 1.70 ± 0.08 mm (FWHM), respectively, as compared to 1.63 ± 0.03 mm (FWHM) when the MPPC-PET module was outside the MRI. Similar results were found for *y*-direction image. Conversely, the signal-to-noise ratio (SNR) of the MR images was only degraded by 5% when the MPPC-PET detector was used.

We next developed a new MRI-PET gantry consisting of eight modules of 4×4 MPPC arrays, coupled with Ce:LYSO scintillator array of 16×16 matrices of $0.5 \times 0.5 \times 10$ mm^3 pixels. The overall geometry of the gantry is actually very similar to that shown at the top of Fig. 4, but all the detector packages are fabricated from acrylonitrile butadiene styrene (ABS) resins rather than metal. Fig. 5 compares the various PET images taken under a static magnetic field (*top left*) with those obtained under FSE (*top center*) and GE (*top right*) operation. The bottom of Fig. 5 compares MR images taken without a PET detector (*bottom left*) with those obtained using PET inside the MRI but with the power turned off (*bottom center*), and with PET inside the MRI but with the power turned on (*bottom right*). It can be seen that no significant interference is confirmed between the MRI and PET images, even under a strong magnetic field of 4.7 T. The MRI-PET data is still being analyzed, Ref. [18] gives full details on this.

3.3. Fast analog ASIC for TOF-PET

To maximize the timing properties of MPPC for future TOF-PET system, we are developing a front-end ASIC with TOF measurement capability in conjunction with a MPPC-array. Our first product (MPPC32) was realized in TSMC 0.35 μm CMOS technology [19]. The circuit comprises 32-ch, low impedance CMOS current conveyors to effectively acquire fast MPPC signals. MPPC32 recorded a coincidence timing resolution of 491 ps (FWHM) as measured between two MPPC pixels (3×3 mm) coupled with a Ce:LYSO crystal ($3 \times 3 \times 10$ mm^3). The energy resolution thus obtained was 10.5% (FWHM) for 511 keV gamma rays. In fact, timing spectra were clearly resolved for a ^{22}Na point source situated at positions spaced 80 mm apart, which confirmed < 500 ps resolution [19]. However, this MPPC32-ASIC could only output one OR-ed analog signal for 32 input channels and, therefore, requires revision for actual use in TOF-PET scanners.

Fig. 6 shows the circuit diagram of the second ASIC-MPPC16 [20]. The most significant change is that the ASIC can independently output 16 ch signals corresponding to each input channel, with power consumption of 28 mW/ch. Similar to MPPC32, the chip consists of two different systems (16-ch CHAIN1 and 1-ch CHAIN2), where CHAIN1 consists of a current conveyor, leading-edge comparator and timing discrimination circuits. Timing can be measured using a sharp leading-edge signal. We used a picosecond light pulser to achieve 105 ps (FWHM) on average for each

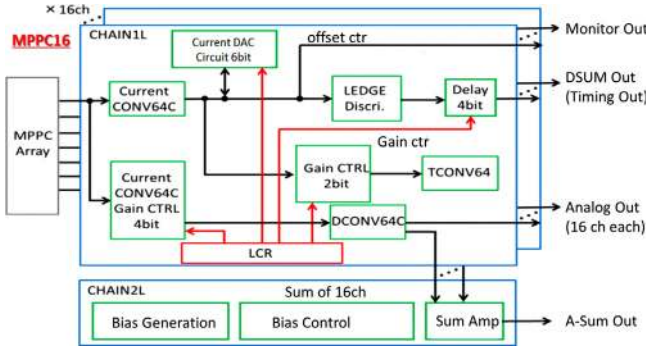

Fig. 6. Circuit diagram of ASIC MPPC16. Two different systems (CHAIN1 and CHAIN2) coexist.

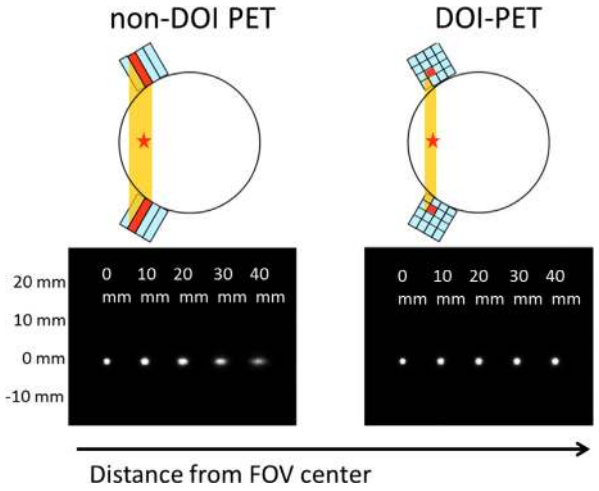

Fig. 7. Schematic concept of non-DOI and DOI PET detectors, and simulated image of a ^{22}Na point source as a function of radial distance from the center of the field of view.

channel in the time jitter measurements. A TOF measurement using back-to-back 511 keV signals from two 16 ch MPPC arrays coupled with Ce:LYSO crystal arrays achieved TOF resolution of 489 ps (FWHM; sum of 16 ch). The energy resolution for the 511 keV signal was 13.7 ± 1.8% (FWHM) on average.

3.4. DOI-PET module

The final key element necessary to achieve the next-generation PET system is the measurement of the DOI of incident gamma rays in the scintillators. As schematically shown in Fig. 7, the point spread function degrades substantially for far-axis positions without DOI information, but such image distortion is prevented in the DOI-PET system. Several ideas and designs for providing DOI information over the total detector volume free of parallax errors have been proposed, especially for Si-PM based PET scanner (e.g. [21–24]). Here, we propose a new DOI-PET system based on 3D segmented scintillators coupled with double-sided MPPC arrays. Ref. [25] gives full details of the design and experimental setup. In short, we can measure the DOI of incident gamma rays by measuring the pulse height ratio of double-sided MPPC arrays consisting of 4×4 channels coupled at both ends of a scintillator block (see the top left of Fig. 8 for a schematic view).

A $BaSO_4$ reflector (0.2 mm thick) divides each pixel of the crystal block (a 2 mm cubic) in the 2D (x–y) direction, whereas the crystal block is separated by a layer of air (approximately 10 μm−thick) in the z-direction, which forms naturally when the pixels are placed on top of each other. The top right of Fig. 8 shows

a photo of the DOI module thus produced; the bottom shows the resultant position response of a performance test for the $4 \times 4 \times 4$, $5 \times 5 \times 5$, and $10 \times 10 \times 10$ matrices of 3 mm cubic, 2 mm cubic, and 1 mm cubic Ce:GAGG crystal pixels, respectively, as measured for 662 keV fully absorbed gamma rays. The energy resolution of each crystal block is typically 8–10% (FWHM) for 662 keV gamma rays. Note that each crystal block is clearly resolved and functions as a high-resolution 3D position-sensitive detector.

4. Compton camera for Fukushima

The thin and compact MPPC is also a key component in a novel Compton camera we are developing in conjunction with Hamamatsu. The camera weights only 1.9 kg and is approximately $\sim 14 \times 14 \times 15$ cm^3 in size [26,28]. It utilizes the kinematics of Compton scattering to contract the source image without using mechanical collimators or coded masks, and also features a wide field of view [27,28]. In order to achieve high sensitivity, the scatterer and absorber must be placed close together, which makes the use of thin MPPC arrays rather than bulky PMTs a significant advantage. Fig. 9 shows the internal structure of the prototype Compton camera developed in 2013. Both the scatterer and absorber consist of 2×2 blocks of 15×15 arrays of $1.5 \times 1.5 \times 5$ mm^3 and $1.5 \times 1.5 \times 10$ mm^3 Ce:GAGG scintillator pixels, respectively, which are optically coupled with 8×8 MPPC-array. The distance between the scatterer and the absorber is set to 15 mm. To reduce the number of output signal channels, we applied a charge division technique based on a newly developed resistor network [6,28]. As detailed in Refs. [26,27] the camera already achieves angular resolution of $\Delta\theta \simeq 13$–14° (FWHM) and energy resolution of 9% (FWHM) as measured for 662 keV gamma rays.

This first prototype has already been tested many times in Fukushima. Fig. 10 shows a sample spectrum (2D energy map comparing the energy deposit in scatter E_1 and absorber E_2) and images taken in a field test conducted on May 30, 2013 [27]. The

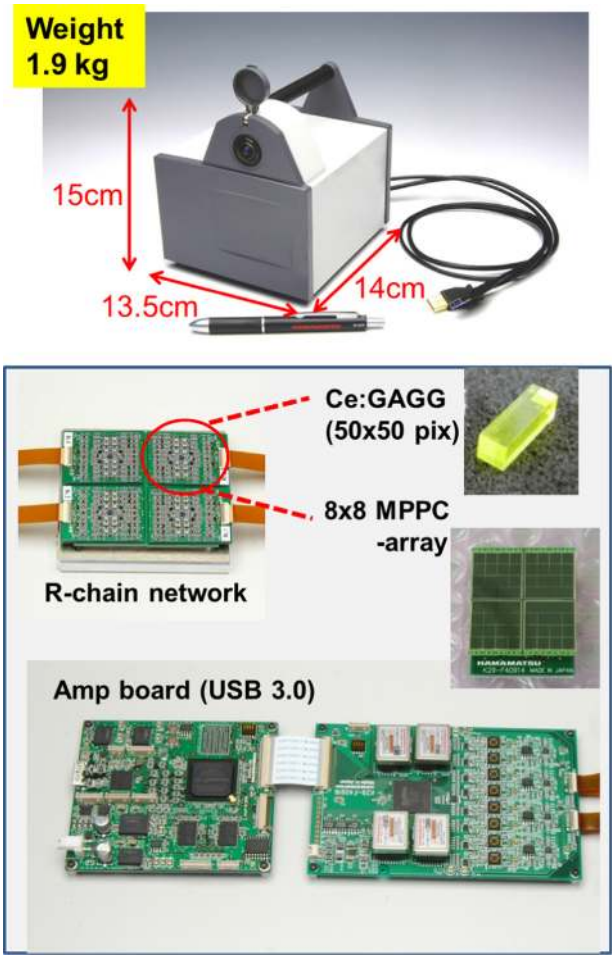

Fig. 9. (*Top*) Photo of Compton camera prototype being fabricated by Hamamatsu. (*Bottom*) Internal structure of prototype Compton camera, consisting of MPPC array, Ce:GAGG scintillators, resistive charge division network, and signal readout boards.

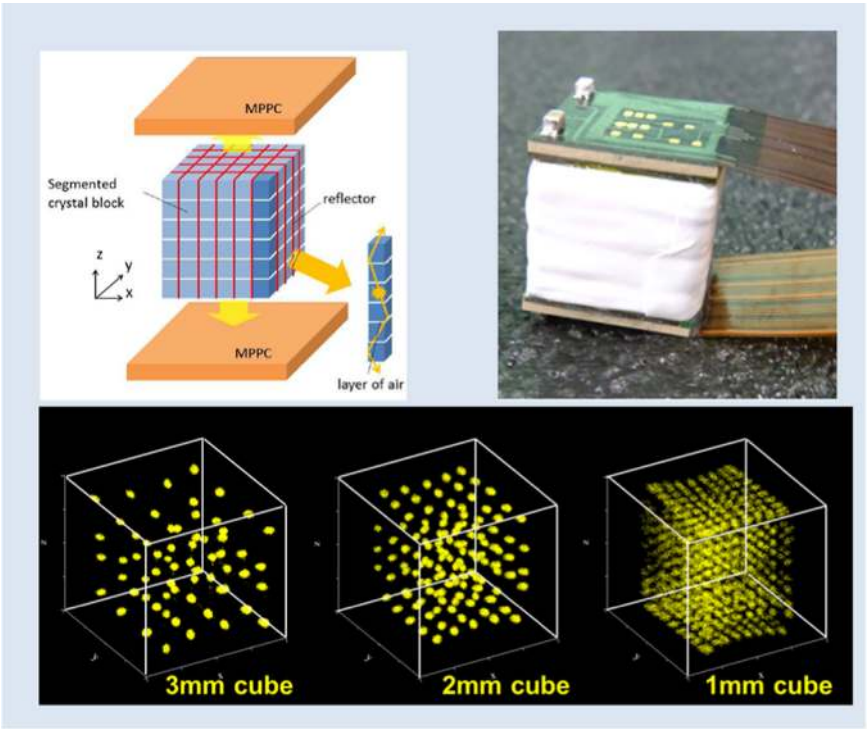

Fig. 8. (*Top*) Schematic illustration and photo of our DOI-PET detector. (*Bottom*) 3D position histogram obtained with $4 \times 4 \times 4$, $5 \times 5 \times 5$, and $10 \times 10 \times 10$ matrices of 3 mm cubic, 2 mm cubic, and 1 mm cubic Ce:GAGG crystal pixels, respectively.

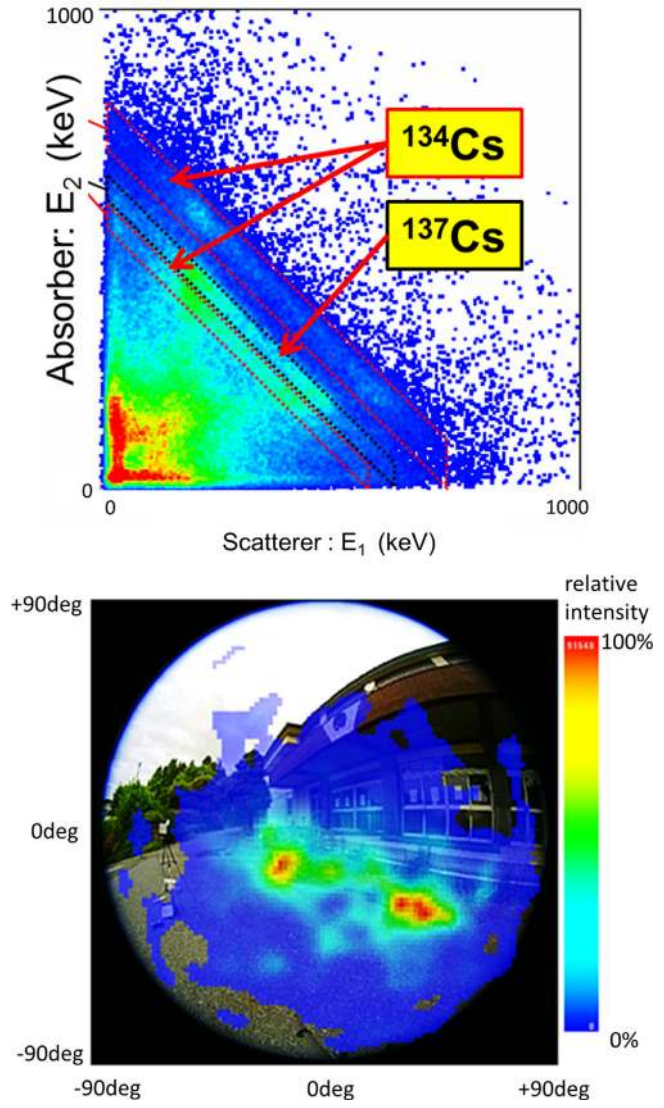

Fig. 10. (*Top*) 2D-map of energy deposits in the scatterer E_1 and absorber E_2, taken during the field testing at Fukushima. Gamma-ray lines from ^{134}Cs (605 keV, 796 keV) and ^{137}Cs (662 keV) are clearly distinguished. (*Bottom*) Sample image taken with this camera with 5-min integration time.

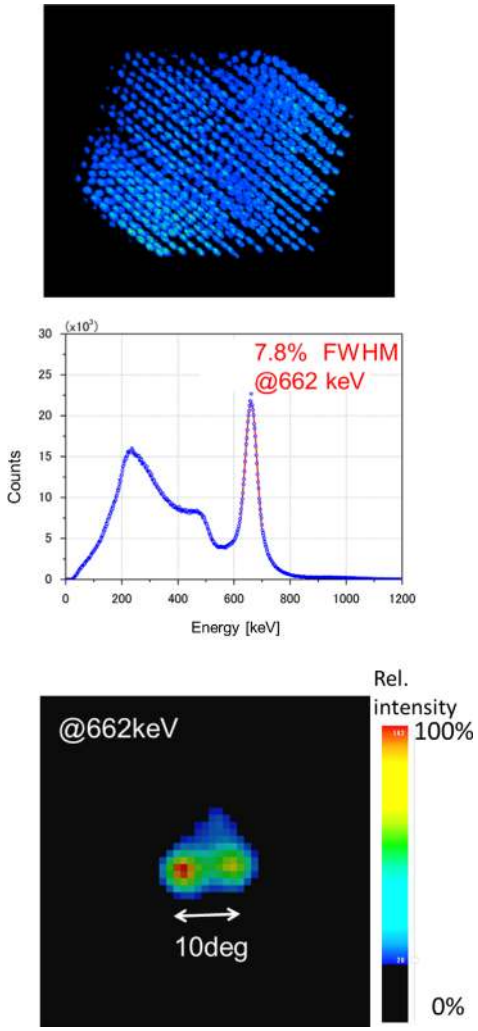

Fig. 11. (*Top*) 3D-position map taken with DOI-Compton camera. (*Center*) Energy spectra summed over absorber, achieving 7.8% (FWHM) resolution at 662 keV. (*Bottom*) Test image taken with two ^{137}Cs isotopes placed 10° apart, confirming improved angular resolution of $\Delta\theta \simeq 8°$.

2D energy map clearly indicates different contributions from ^{134}Cs (605 keV, 796 keV) and ^{137}Cs (662 keV), as indicated by dotted lines falling to the right. The bottom image was taken within 5 min only, with selection criteria of 10 keV $< E_1 <$ 165 keV, and 612 keV $< E_1 + E_2 <$ 712 keV. The maximum likelihood-expectation maximization (MLEM) algorithm in the list-mode was applied to the image. Various field tests conducted in Fukushima have verified the performance of this useful Compton camera, which is now ready for use in decontamination operations. By applying the triangular surveying method, we are also proposing a new concept for the stereo measurement of gamma ray using multiple Compton cameras [29,30].

As the next step, we are developing a DOI-Compton camera by applying newly developed technology as described in Section 3.4. By measuring pulse-height ratio of MPPC arrays coupled at both ends of scintillator block, the 3D position of the gamma-ray interaction (i.e., scattering and absorbing positions) can be precisely determined with an accuracy of 2 mm (FWHM) [9]. This results in a significant improvement in angular resolution to $\Delta\theta \sim 8°$ (FWHM) at 662 keV. Fig. 11 shows the 3D position map, energy spectrum and first experimental image of the device. Two isotopes (^{137}Cs; 0.5 and 1 MBq level) placed 10° apart are clearly resolved within the image. Ref. [31] gives full details on the performance of the DOI-Compton camera, comparing the image quality taken with non-DOI and DOI Compton cameras in a field test conducted at Fukushima in July 2014. Further challenges regarding the use of the Compton camera for real-time monitoring of prompt gamma-ray emission during proton therapy and for the production of advanced SPECT image will be given elsewhere.

5. Conclusion

In this paper, we briefly summarized the highlights and most recent progress of MPPC-based scintillation detectors. We focused on three examples: (1) a high-precision X-ray and gamma-ray spectral image sensor, (2) next-generation PET detectors having MRI, TOF, and DOI measurement capabilities, and (3) a compact gamma camera for environmental radiation surveys, especially for use at Fukushima. We showed that a simple configuration of a diced scintillator plate coupled with a large-area MPPC array acts as a convenient "multi-color" imager that may be potentially useful for future SPECT and photon-counting CT. A prototype system for a high-resolution, MPPC-based PET scanner showed $\simeq$ 1 mm (FWHM) spatial resolution, even under a strong magnetic

Please cite this article as: J. Kataoka, et al., Nuclear Instruments & Methods in Physics Research A (2014), http://dx.doi.org/10.1016/j.nima.2014.11.004

field of 4.7 T. We also reported on a front-end ASIC intended for future TOF-PET scanners, and a novel design for a MPPC module with DOI measurement capability. Finally, we presented the concept of a two-plane Compton camera consisting of Ce:GAGG scintillator arrays coupled with thin MPPC arrays. The latest Compton camera products developed in conjunction with Hamamatsu achieve excellent sensitivity and angular resolution of $\Delta\theta\sim 8^{\circ}$ (FWHM) at 662 keV by employing DOI-segmented scintillator arrays. These results suggest that the MPPC is a promising light sensor for next-generation radiation detectors as detailed in the paper.

References

[1] K. Yamamoto, et al., IEEE Nuclear Science Symposium Conference Record, vol. N30-102, 2006, p. 1094.
[2] P.P. Webb, R.J. McIntyre, J. Cornadi, RCA Review 35 (1974) 234.
[3] J. Kataoka, et al., Nuclear Instruments and Methods in Physics Research Section A 541 (2005) 398.
[4] T. Tsujikawa, et al., Nuclear Instruments and Methods in Physics Research Section A 765 (2014) 247.
[5] T. Kato, et al., Nuclear Instruments and Methods in Physics Research Section A 638 (2011) 83.
[6] T. Nakamori, et al., Journal of Instrumentation 7 (2012) C01083.
[7] T. Kato, et al., Nuclear Instruments and Methods in Physics Research Section A 699 (2013) 235.
[8] K. Yamamoto, et al., Nuclear Instruments and Methods in Physics Research Section A 732 (2013) 547.
[9] D.J. Hall, et al., Nuclear Instruments and Methods in Physics Research Section A 678 (2012) 64.
[10] J. Kataoka, et al., IEEE Transactions on Nuclear Science NS-57 (2010) 2448.
[11] S. Yamamoto, et al., Physics in Medicine and Biology 55 (2010) 5817.
[12] R. Pani, et al., Nuclear Instruments and Methods in Physics Research Section A 513 (2003) 36.
[13] W. Xi, et al., Nuclear Medicine and Biology 37 (2010) 24.
[14] T. Fujita, et al., Nuclear Instruments and Methods in Physics Research Section A 765 (2014) 262.
[15] S. Yamamoto, et al., Physics in Medicine and Biology 56 (2011) 4147.
[16] S. Yamamoto, et al., Physics in Medicine and Biology 58 (2013) 7875.
[17] Y. Kurei, et al., Nuclear Instruments and Methods in Physics Research Section A 765 (2014) 275.
[18] Y. Kurei, et al., Journal of Instrumentation, 2014, in press.
[19] H. Matsuda, et al., Nuclear Instruments and Methods in Physics Research Section A 699 (2013) 211.
[20] T. Ambe, et al., Nuclear Instruments and Methods in Physics Research Section A, 2014, in press.
[21] E.P. Delifino, et al., IEEE Transaction on Nuclear Science Symposium Conference Record, 2010, p. 3442.
[22] P. Dokhale, et al., IEEE Nuclear Science Symposium Conference Record, 2009, p. 2809.
[23] F. Taghibakhsh, et al., IEEE Nuclear Science Symposium Conference Record, 2009, p. 2821.
[24] N. Inadama, et al., IEEE Transactions on Nuclear Science NS-61 (2014) 53.
[25] A. Kishimoto, et al., IEEE Transactions on Nuclear Science NS-60 (2013) 38.
[26] J. Kataoka, et al., Nuclear Instruments and Methods in Physics Research Section A 732 (2013) 403.
[27] T. Nishiyama, et al., IEEE Nuclear Science Symposium Conference Record, NSSMIC.2013.6829417, 2013.
[28] H. Suzuki, et al., IEEE Nuclear Science Symposium Conference Record, NSSMIC.2013.6829610, 2013.
[29] K. Takeuchi, et al., IEEE Nuclear Science Symposium Conference Record, NSSMIC.2013.6829615, 2013.
[30] K. Takeuchi, et al., Nuclear Instruments and Methods in Physics Research Section A 765 (2014) 187.
[31] A. Kishimoto, et al., Journal of Instrumentation, 2014, in press.

Please cite this article as: J. Kataoka, et al., Nuclear Instruments & Methods in Physics Research A (2014), http://dx.doi.org/10.1016/j.nima.2014.11.004